International Journal of Safety and Security Engineering
Vol. 14, No. 4, August, 2024, pp. 1319-1329
Journal homepage: http://iieta.org/journals/ijsse

Response of Anchored and Embedded Reinforced Concrete Barriers Subjected to Blast Loads

Amira Elyamany[1*], Walid A. Attia[2]

[1] PhD Candidate, Structural Engineering Department, Cairo University, Giza 12613, Egypt
[2] Professor of Structural Analysis and Mechanics, Structural Engineering Department, Cairo University, Giza 12613, Egypt

Corresponding Author Email: amira.elyamany.n@eng-st.cu.edu.eg

https://doi.org/10.18280/ijsse.140428

Received: 23 June 2024
Revised: 23 July 2024
Accepted: 9 August 2024
Available online: 30 August 2024

Keywords:
blast loads, reinforced concrete barriers, ANSYS AUTODYN 18.2, explicit dynamics, TNT, standoff distance

ABSTRACT

Protecting important buildings and preserving human lives is an essential requirement in present era as explosions represent a real danger which must be confronted. Current study analyzes the behavior of different eight (8) reinforced concrete barriers subjected to blast loads. The models are divided into barriers anchored in the base and barriers with a base embedded into soil. In addition, the models feature different geometries as there are concave barriers with front angles 49° and 58°. Also, different weights of TNT charges 450 kg, and 1800 kg are used. The study concluded that anchored barriers subjected to TNT charge of 450 kg, barriers with a front angle 49° have the best performance in terms of the pressure values behind the barrier. These barriers have approximately 61% lower pressure values at the center point of barrier back compared to other types of barriers. The best performance is for barrier with front angle 58° in case of TNT charge weighted 1800 kg. These barriers have approximately 41% lower pressure values at the bottom point of the barrier back compared to other types of barriers. In case of embedded barriers, the performance of barriers having front angle 58° is better than the other barriers in case of TNT charge of 450kg. These barriers have approximately 49% lower pressure values at the center point of barrier back compared to other types of barriers. In case of TNT charge of 1800kg the best performance was for barriers having front angle 58°. These barriers have approximately 52% lower pressure values at the center point of barrier back compared to other types of barriers. Overall, the embedded barriers demonstrate a better performance rather than the anchored barriers across all TNT charges from pressure values behind the barrier perspective.

1. INTRODUCTION

Explosions pose a great threat to safety of human lives and structures. Some structures, such as sensitive governmental facilities, archaeological sites, and important structures near petrochemical facilities should have protection systems designed to withstand blast loads. Reinforced concrete barriers are used in order to protect these structures. The current study sheds light on two approaches to enhancing the performance of barriers, such as anchoring the barriers at the base and embedding the barriers into soil. Both approaches are effective, economical and feasible. On the other hand, this study paves the way for other researchers to use similar approaches with different geometries, software and end conditions.

2. LITERATURE REVIEW

Wu et al. [1] performed a study at which 16 tests were executed on RC slabs with the same reinforcement ratio but different reinforcement distribution and the same scale distance but different blast distances. The tests were carried out on 8 models of single layer reinforcement slabs and 8 models of double layer reinforcement slabs. The results show that damage area of the bottom face of single-layer reinforcement was 1.8-34.1% greater than that of double layer. When the blast distance was small, the peak displacement of single layer reinforcement was larger than the double layers by 2.8-22.6%. When the blast distance was large, the peak displacement of double-layer reinforced slabs was larger than single layer by 10.1-29.3%.

Mai et al. [2] carried out a study in which various Ultra-high Performance Fiber Reinforced Concrete panels, with 158MPa compressive strength, were analyzed due to the effect of blast load. Panel with dimension 3.5×1.3 m is subjected to 100 kg TNT charge. The thickness of panel varies between 150 mm, 120 mm, 100 mm and 80 mm. The maximum observed deflection = 262.8 mm, and 45.70 mm for 80 mm panel thickness and 150 mm panel thickness respectively. The standoff distance varies between 9 m, 7 m and 12 m. The maximum observed deflection was 554 mm, and 146 mm for standoff distance 7 m and 12 m respectively. Also, the reinforcement ratio varies between 3.4%, 1.7%, 1%, and 0.3%. The observed deflection in case of 3.4% reinforcement ratio and 0.3% is 49.90 mm and 68.30 mm respectively.

Park et al. [3] performed a study to investigate the resistance

of storage tanks consisted of two walls, a roof and a raft under a TNT charge weighing 5.90 kg. The tanks were tested in different conditions such as fully vented, fully confined and partially confined using normal concrete strength (26.70 MPa) and high concrete strength (100.80 MPa). The study concluded that under a fully confined explosion, the displacements were extremely high in contrast to fully vented explosions. Also, under a partially confined explosion, the use of high strength concrete reduced the maximum displacement by 98.70%.

Attia et el. [4] carried out a study to investigate the relationship between barrier geometry and blast wave propagation. Consequently, 9 reinforced concrete barriers with variable geometry were subjected to 50 kg and 400 kg TNT charges. The standoff distance of TNT is 2 m. The barrier geometries included three types: the first type was a concave face with convex back, the second type was a concave face with planar back, and the third type was a hunched base with planar back. For the first group, the results showed that the pressure ranged between 1×10^4 kPa at 2.70 ms in case of 50 kg TNT and 4×10^4 kPa at 2.50 ms. For the second group, the results showed that the pressure ranged between 1×10^4 kPa at 1.80 ms in case of 50kg TNT and 4×10^4 at 1.40 ms. For the third group, the results showed that the pressure ranged between 0.80×10^4 kPa at 1.80 ms for 50kg TNT and 0.60×10^4 kPa at 4.30 ms. Previous studies have investigated different reinforcement distribution [1], various ultra-high performance fiber reinforced concrete panels [2], different confinement conditions [3], and variable geometries with varying TNT charge weights [4]. However, none of these studies involved anchoring the base to the wall or embedding the base in the soil.

3. BLAST PHENOMENA

When detonation occurs, it leads to the propagation of high pressure which produce shock wave called blast wave. The blast wave pressure changes after detonation from ambient pressure P_o at time t_A to peak pressure P_{so}. After time t_A+t_d, the pressure returns to P_o, at which the positive phase is finished and the negative phase starts. The negative phase finishes at time (t_{d^-}), and the pressure reaches (P_{so^-}). Figure 1 below shows the different stages of detonation time and corresponding pressure changes.

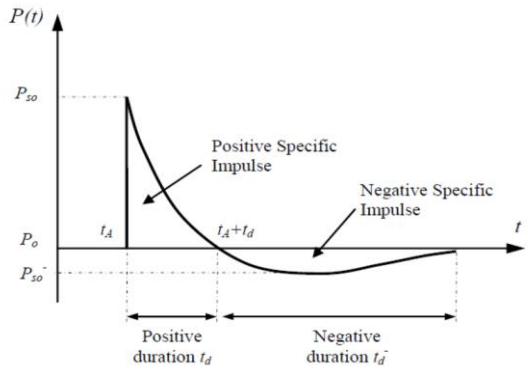

Figure 1. Typical pressure-time history of blast load [5]

Sadovskiy [6] proposed the following equation to estimate the time duration of positive overpressure.

$$t_{pos} = 1.2\sqrt[6]{W}\sqrt{R}\ (\text{ms})$$

Krauthammer and Altenberg [7] proposed the following equations to calculate time duration of negative pressure:

$$t_{neg} = 0.0104W^{1/3}\ sec.(Z < 0.30) \quad (1)$$

$$t_{neg} = (0.003125\ log_{10}Z + 0.01201)W^{\frac{1}{3}}\ sec. \quad (1.9 > Z > 0.3) \quad (2)$$

$$t_{neg} = 0.0139\ W^{1/3}\ sec.(Z > 1.9) \quad (3)$$

where, Z: as per Hopkinson [8] and Cranz et al. [9]: The scaled distance, with units ($m/kg^{1/3}$):

$$Z = \frac{R}{W^{\frac{1}{3}}} \quad (4)$$

where, R: The range from the center of the charge (m); W: The mass of TNT charge (kg).

4. THEORITECAL BASIS OF ANSYS AUTODYN ANALYSIS

ANSYS AUTODYN is a finite element analysis tool developed by ANSYS, Inc., an American company. This tool was developed to model and solve nonlinear explicit dynamics of gases, fluids and solids along with their interactions.

The calculation procedures are made through many different discretization methods for numerical formulations: Eulerian, Lagrangian, Arbitrary Lagrange-Euler (ALE) [10], and Smoothed Particle Hydrodynamics [11], each one of these methods can be used separately; however, complex problems may require the use of a combination of them. The Lagrange method is used to divide solid objects. The objects are divided into a mesh of finite elements. The mesh nodes move and deform simultaneously, with no overlap movement between nodes. This method can be used perfectly to simulate the boundaries which divide different materials and surfaces. The Euler method is used to spatial fluids, and gases where the whole mesh is solved as a region. The nodes of this mesh are fixed in space. This method is suitable to simulate the liquids and gases during impacts or explosion events. The Arbitrary Lagrange Euler (ALE) calculation method combines the best aspects of the two previous methods. The user specifies how the finite element mesh can move and deform either free as Lagrange or fixed as Euler. This method prevents the mesh distortion occurs during the simulation. The SPH method is used to simulate the impact of objects composed of brittle materials.

5. METHODS

The RC walls and base are modelled using body elements with Lagrange reference frame and flexible stiffness behavior for wall but rigid stiffness behavior for base. Reinforcing steel bars are modelled using beam elements with a Lagrange reference frame and flexible stiffness behavior. For the explosive charge modelling, the weights of the explosive material are modelled using body elements with a Euler reference frame with flexible stiffness behavior. Air material is modelled using body elements with a Euler reference frame with flexible stiffness behavior. The used mesh size is 0.10 m.

The concrete material used in the AUTODYN model representation of the wall barriers has a unit weight of 2.75 t/m³ and a characteristic strength of 35 MPa [12].

The steel material used in the AUTODYN model representation of the wall barriers reinforcement has a unit weight of 7.83 t/m³ and yield stress of 400 MPa [13].

TNT explosive material will be used as the primary source of explosion energy [14]. High explosives are typically represented using the Jones-Wilkins-Lee (JWL) EOS to simulate the pressure generated energy that resulted in an explosion [15, 16].

The soil was modeled using Drucker-Prager strength linear method [17-19].

The current study discusses 8 models of reinforced concrete barriers subjected to blast loads, analyzed using ANSYS AUTODYN 18.2 software. The study is based on two groups of reinforced concrete barriers.

The first group consists of two types of geometry:

Type -1: Curved wall with concave front angle 49° which is opposite to TNT charge

Type -2: Curved wall with concave front angle 58° which is opposite to TNT charge

The common factor between the two types that the wall (1m width) is connected to rigid base raft (8 m length × 2 m width) with L-shaped steel reinforcement anchors. TNT charge is positioned at a standoff distance 1.00 m from the walls. Different TNT charges weights is utilized 450 kg, 1800 kg to represent respectively van/SUV, small moving van/delivery truck that carry an explosive [20]. The estimated time of explosion is calculated as per previous equations from Eqs. (1) to (4). The walls naming is as following:

For type-1: AN-49-1-450, and AN-49-1-1800

For type-2: AN-58-1-450, and AN-58-1-1800

The barriers geometry is as following Figure 2 and Figure 3:

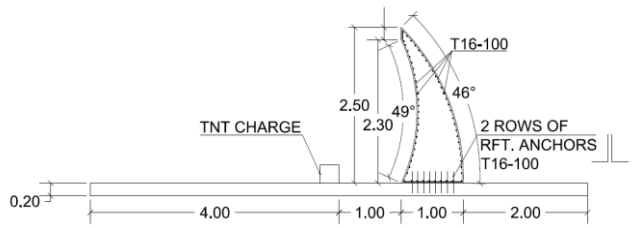

Figure 2. Type (1) barrier walls

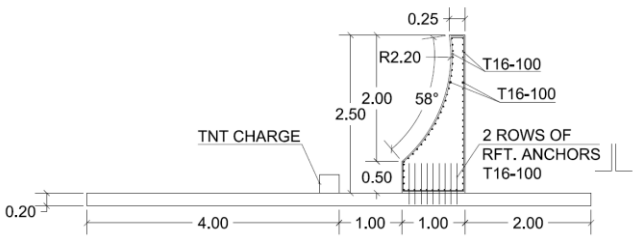

Figure 3. Type (2) barrier walls

The second group also has the same two types of geometry and the common factor between the two types that the raft (8 m length × 2 m width) is embedded under soil by 0.40m. TNT charge is positioned at a distance 1.00 m from the walls. Different TNT charges weights is used 450 kg and 1800 kg. The walls naming is as following:

Type-3: EM-49-1-450, and EM-49-1-1800

Type-4: EM-58-1-450, and EM-58-1-1800

The barriers geometry is as following Figure 4 and Figure 5:

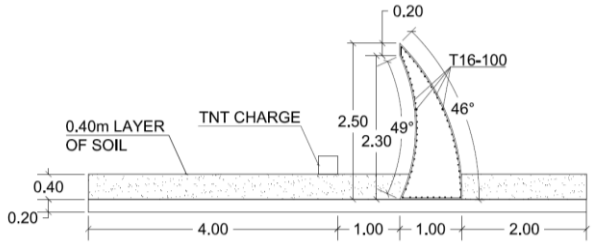

Figure 4. Type (3) barrier walls

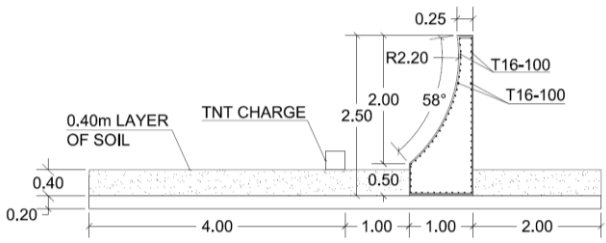

Figure 5. Type (4) barrier walls

6. RESULTS

6.1 Barriers type (1) and (2) details

The followings points are considered as gauges to measure pressure and displacement in the y (vertical displacement) and z (horizontal displacement) directions. The locations of gauges are illustrated at the Figures 6 and 7.

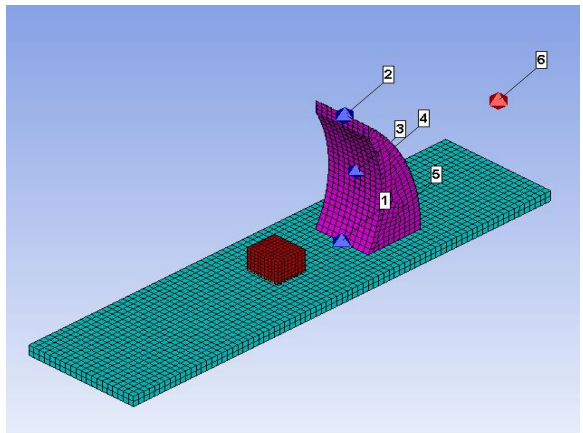

Figure 6. Gauges location of barriers start with AN-49

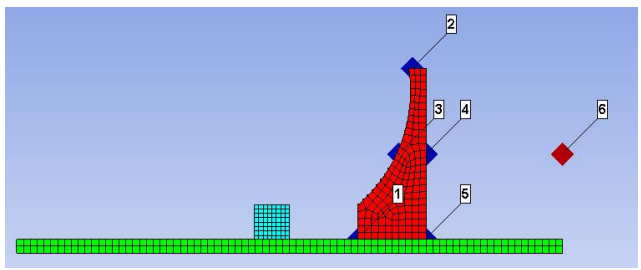

Figure 7. Gauges location of barriers start with AN-58

The following Figures 8 and 9 present the reinforcement configuration which is adopted.

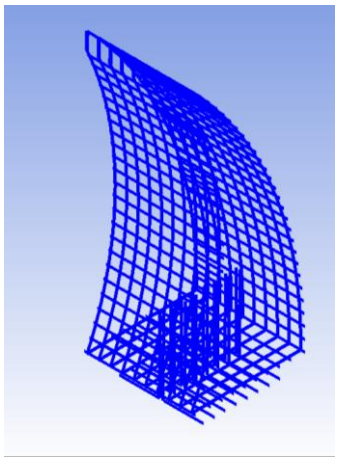

Figure 8. Reinforcement details of barriers start with AN-49

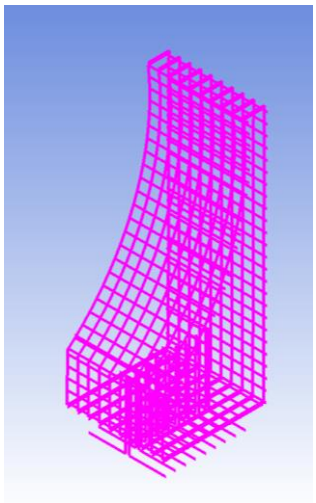

Figure 9. Reinforcement details of barriers start with AN-58

6.2 Barriers type (1) pressure results

The following Figure 10 represents results of pressure contour of the whole configuration at the last cycle due to blast load for type AN-49-1-450 which varies between -5.30*10^3 kPa and 7.26*10^3 kPa.

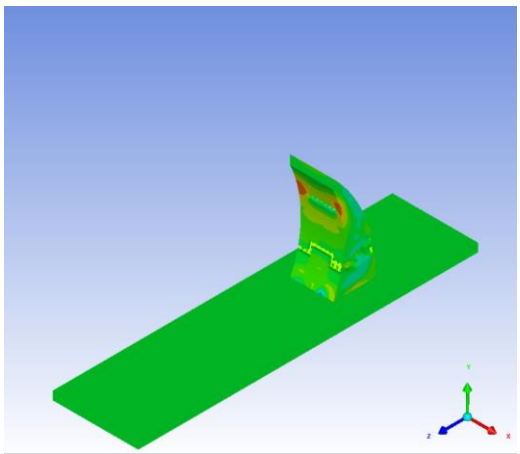

Figure 10. Pressure contour of AN-49-1-450

The following Figure 11 represents results of pressure contour at the last cycle of the whole configuration due to blast load for type AN-49-1-1800 which varies between -5.18*10^3 kPa and 9.29*10^3 kPa.

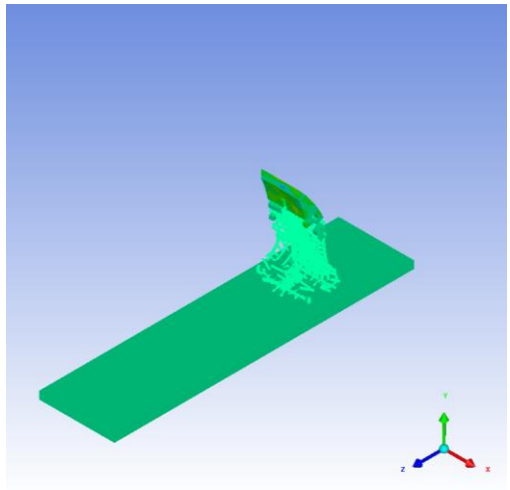

Figure 11. Pressure contour of AN-49-1-1800

Figure 12 represents Pressure-Time history of AN-49-1-450 at gauges points which varies between 2.40*10^3 kPa at gauge 6 and 1.80*10^5 kPa at gauge 1.

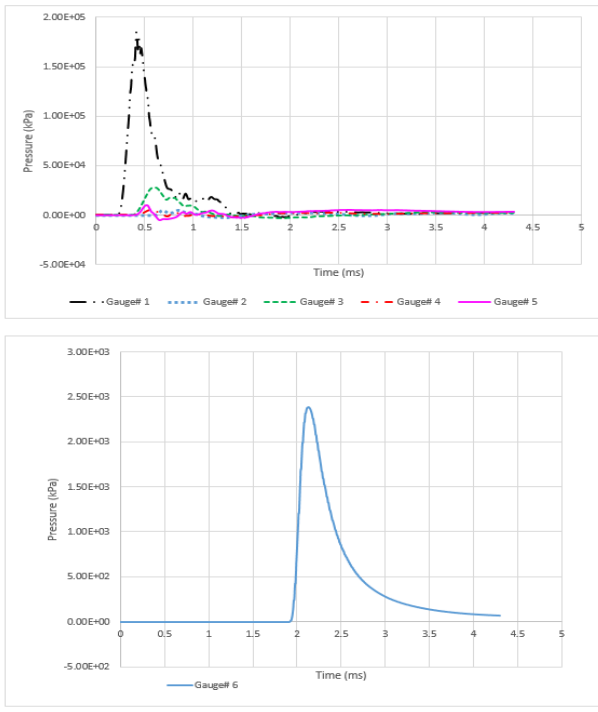

Figure 12. Pressure-Time history of AN-49-1-450

The following Figure 13 represents Pressure-Time history of AN-49-1-1800 at gauges points which varies between 5.00*10^3 kPa at gauge 6 and 6.00*10^5 kPa at gauge 1.

6.3 Barriers type (2) pressure results

The following Figure 14 represents results of pressure contour at the last cycle of the whole configuration due to blast load for type AN-58-1-450 which varies between -6.56*10^3 kPa and 6.40*10^3 kPa.

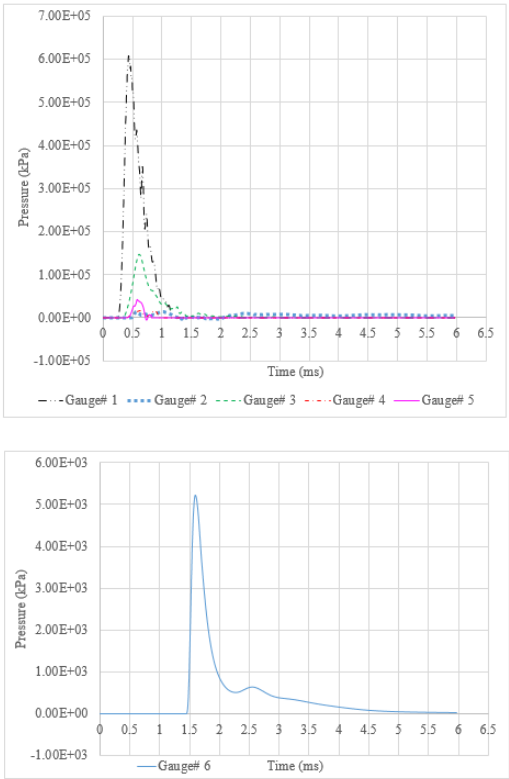

Figure 13. Pressure-Time history of AN-49-1-1800

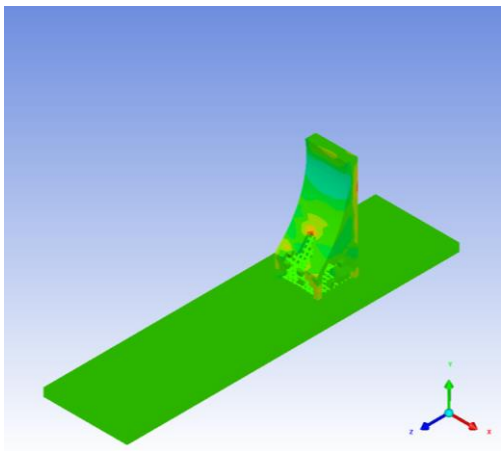

Figure 14. Pressure contour of AN-58-1-450

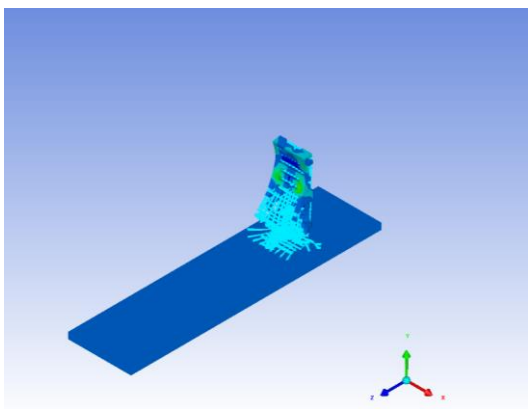

Figure 15. Pressure contour of AN-58-1-1800

Figure 15 represents results of pressure contour at the last cycle of the whole configuration due to blast load for type AN-58-1-450 which varies between -2.53*10^3 kPa and 1.59*10^4 kPa.

The following Figure 16 represents Pressure-Time history of AN-58-1-450 at gauges points which varies between 1.10*10^3 kPa at gauge 6 and 2.00*10^5 kPa at gauge 1.

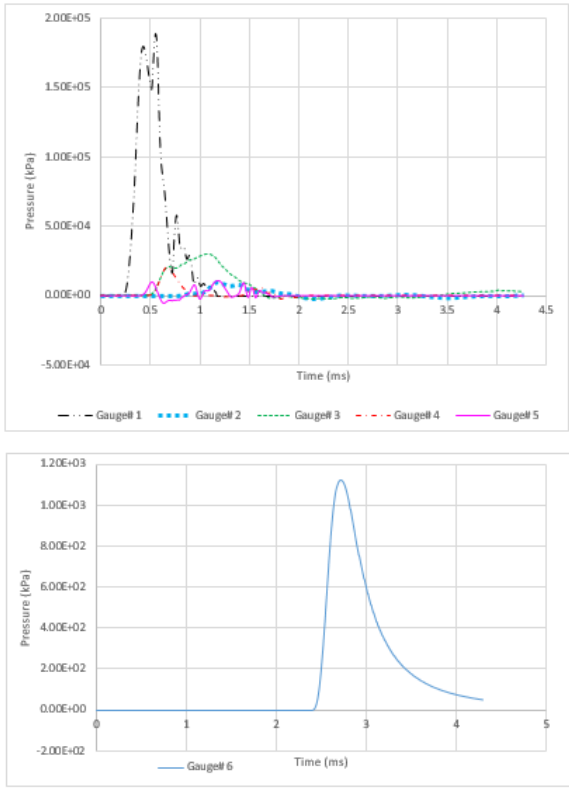

Figure 16. Pressure-Time history of AN-58-1-450

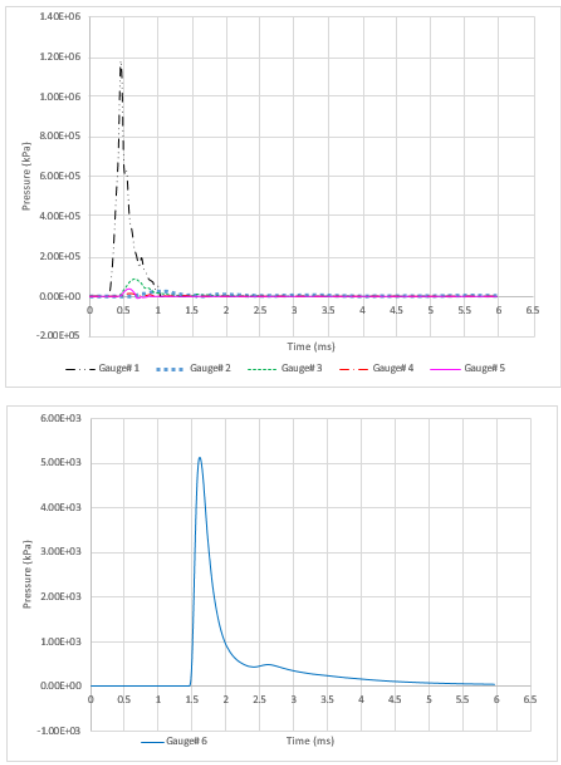

Figure 17. Pressure-Time history of AN-58-1-1800

Figure 17 represents Pressure-Time history of AN-58-1-1800 at gauges points which varies between 5.00*10^3 kPa at

gauge 6 and 1.20*10^6 kPa at gauge 1.

6.4 Barriers type (3) and (4) details

The following Figure 18 shows gauge points which are used for barriers start with EM-49.

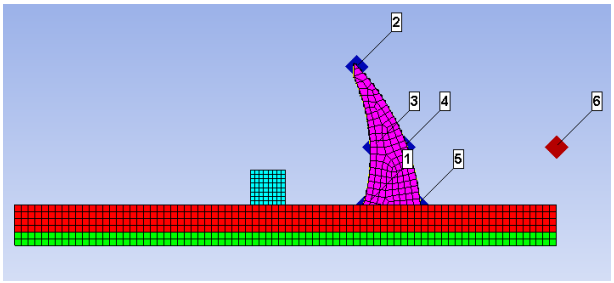

Figure 18. Gauges location of barriers start with EM-49

On the other hand, the following Figure 19 illustrates the location of gauge points which are used in case of barriers start with EM-58.

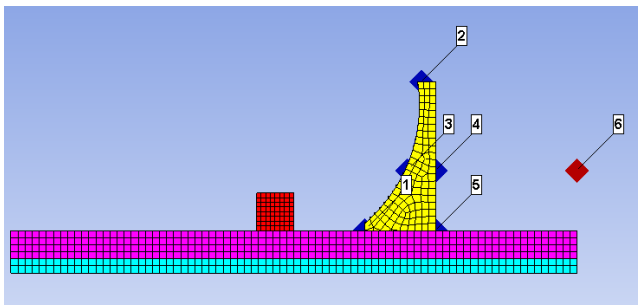

Figure 19. Gauges location of barriers start with EM-58

The following reinforcement configuration is adopted as per Figure 20 for barriers start with EM-49. In addition, Figure 21 demonstrate reinforcement details of barriers start with EM 58.

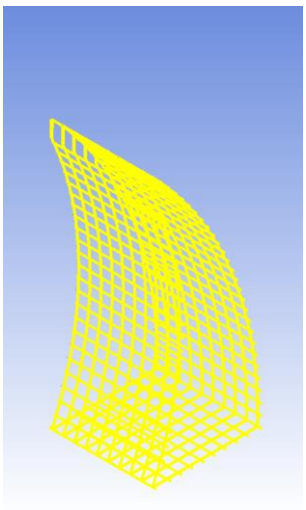

Figure 20. Reinforcement details of barriers start with EM-49

6.5 Barriers type (3) pressure results

The following Figure 22 represents results of pressure contour at the last cycle of the whole configuration due to blast load for type EM-49-1-450 which varies between -3.75*10^5 kPa and 4.54*10^5 kPa.

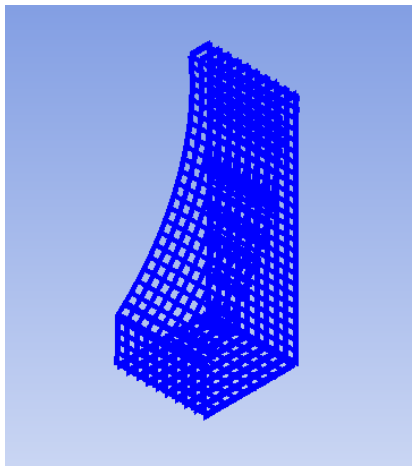

Figure 21. Reinforcement details of barriers start with EM-58

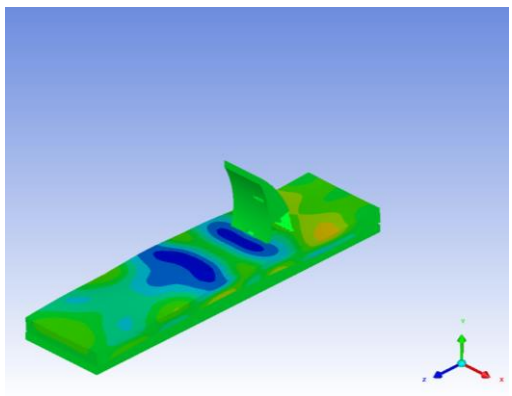

Figure 22. Pressure contour of EM-49-1-450

The following Figure 23 represents results of pressure contour at the last cycle of the whole configuration due to blast load for type EM-49-1-1800 which varies between -5.87*10^5 kPa and 7.92*10^5 kPa.

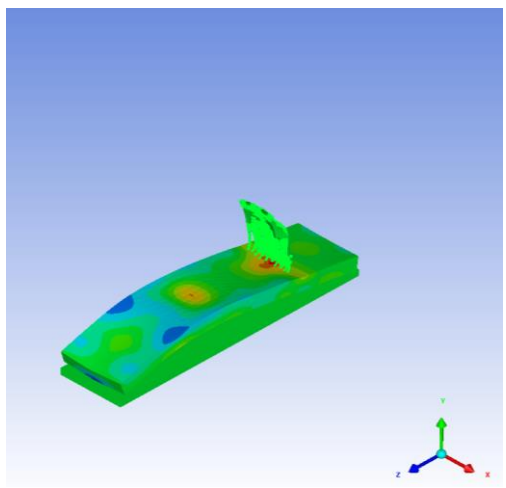

Figure 23. Pressure contour of EM-49-1-1800

The following Figure 24 represents Pressure-Time history of EM-49-1-450 at gauges points which varies between 1.00*10^3 kPa at gauge 6 and 1.40*10^5 kPa at gauge 1.

The following Figure 25 represents Pressure-Time history of EM-49-1-1800 at gauges points which varies between $2.30*10^3$ kPa at gauge 6 and $3.20*10^5$ kPa at gauge 1.

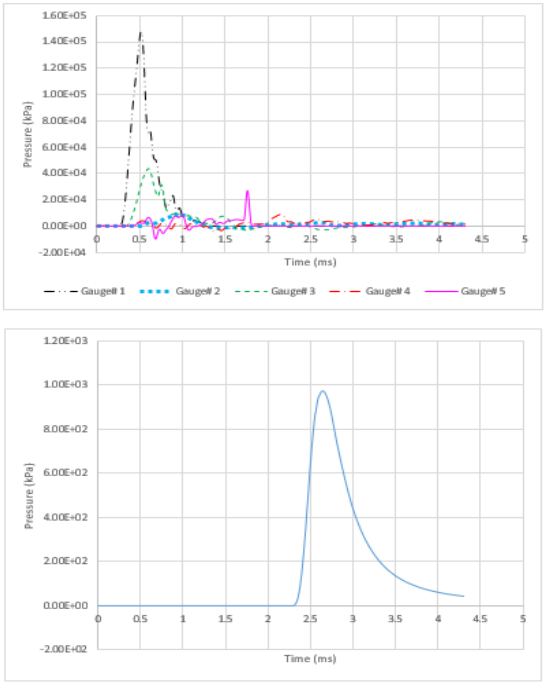

Figure 24. Pressure-Time history of EM-49-1-450

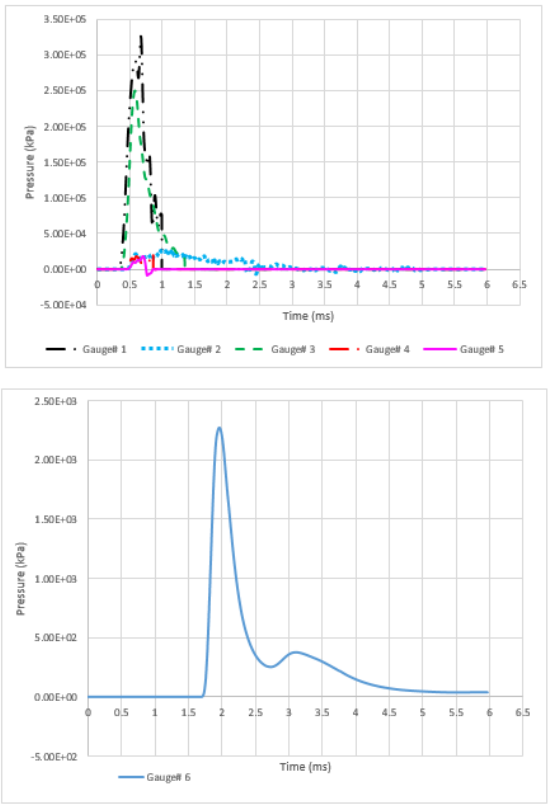

Figure 25. Pressure-Time history of EM-49-1-1800

6.6 Barriers type (4) pressure results

The following Figure 26 represents results of pressure contour at the last cycle of the whole configuration due to blast load for type EM-58-1-450 which varies between $-3.76*10^5$ kPa and $3.92*10^5$ kPa.

The following Figure 27 represents results of pressure contour at the last cycle of the whole configuration due to blast load for type EM-58-1-1800 which varies between $-6.97*10^5$ kPa and $9.36*10^5$ kPa.

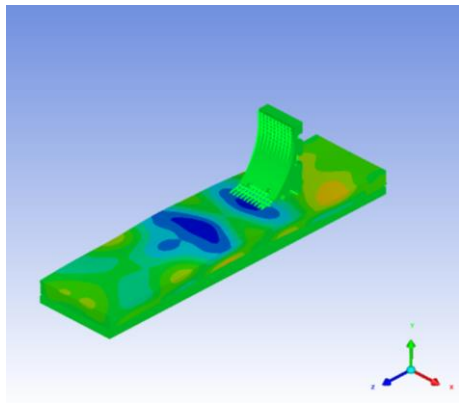

Figure 26. Pressure contour of EM-58-1-450

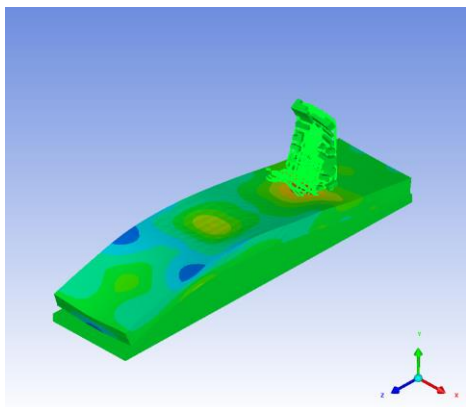

Figure 27. Pressure contour of EM-58-1-1800

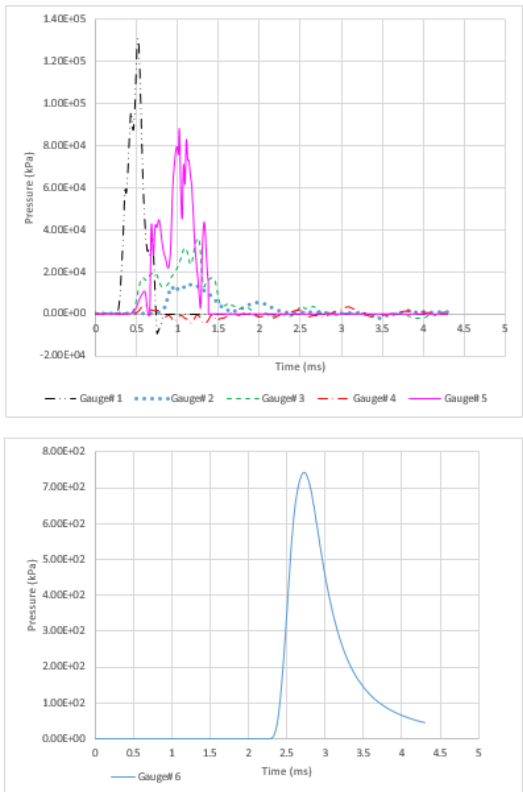

Figure 28. Pressure-Time history of EM-58-1-450

Figure 28 represents Pressure-Time history of EM-58-1-450 at gauges points which varies between $7.20*10^2$ kPa at gauge 6 and $1.30*10^5$ kPa at gauge 1.

The following Figure 29 represents Pressure-Time history of EM-58-1-1800 at gauges points which varies between $1.80*10^3$ kPa at gauge 6 and $2.80*10^5$ kPa at gauge 1.

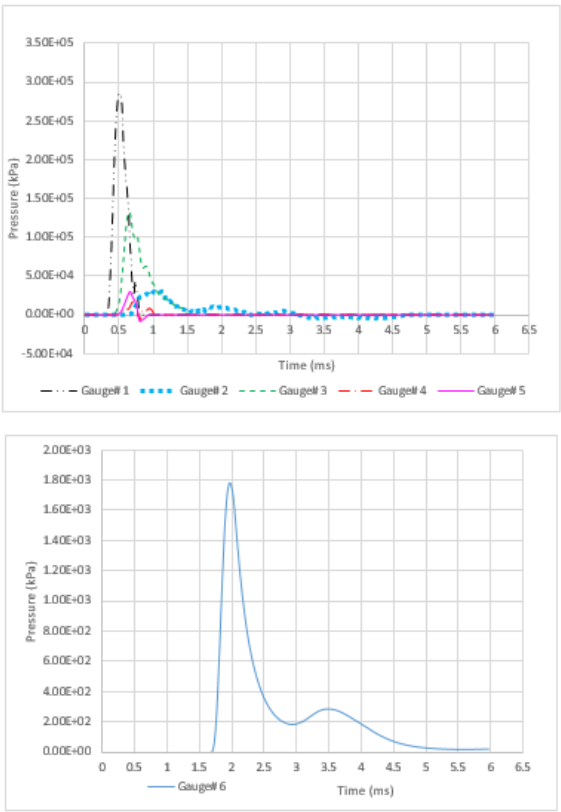

Figure 29. Pressure-Time history of EM-58-1-1800

6.7 Comparative analysis of barriers type (1)

The following results of Table 1 illustrate the max Uy (Vertical displacement) and max Uz (horizontal displacement) obtained from different TNT charges for gauges from no.1 to no.5 as gauge no.6 records very minor displacement values. In addition, Figure 30 compares Uy of different gauges for AN-49-1-450 and AN-58-4-450. In case of Uy (vertical displacement) of type-1 barriers the values of AN-58-1-450 gauges is less than AN-49-1-450 gauges by ratios vary between 3.50% up to 82.90% at different gauges except gauge (2).

Table 1. Uy (vertical displacement) of different anchored barriers due to same TNT charge (450 kg)

	Max Uy (mm)	
Gauge No.	**AN-49-1-450**	**AN-58-1-450**
Gauge-1	5.49	0.93
Gauge-2	12.09	12.24
Gauge-3	10.41	10.05
Gauge-4	15.71	12.91
Gauge-5	12.63	6.86

Also, in case of Uy (vertical displacement) for type-2 barriers the values of AN-58-1-1800 gauges is less than AN-49-1-1800 gauges by ratios vary between 54.20% up to 87.10% at different gauges except gauge (5). The results of Uy are shown in Table 2. Furthermore, Figure 31 compares the results of Uy at different gauges for AN-49-1-1800 and AN-58-1-1800.

On the other hand, in case of Uz (horizontal displacement) for type-1 barriers the values of AN-58-1-450 gauges is less than AN-49-1-450 gauges by ratios vary between 34.90% up to 73.80% at different gauges. Moreover, Table 3 display the results of Uz and Figure 32 compares the results of Uz at different gauges for AN-49-1-450 and AN-58-1-450.

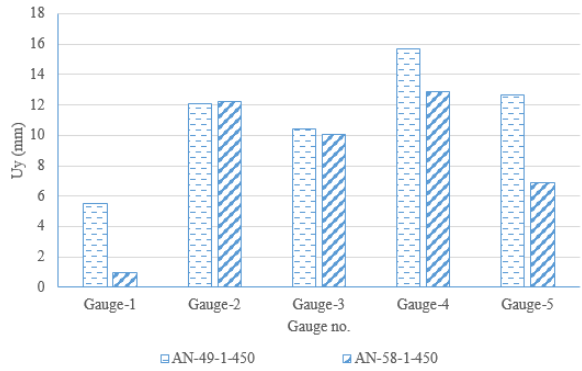

Figure 30. Uy (vertical displacement) of different anchored barriers due to same TNT charge (450 kg)

Table 2. Uy (vertical displacement) of different anchored barriers due to same TNT charge (1800 kg)

	Max Uy (mm)	
Gauge No.	**AN-49-1-1800**	**AN-58-1-1800**
Gauge-1	23.70	10.84
Gauge-2	149.74	0.70
Gauge-3	43.84	5.65
Gauge-4	7.68	1.90
Gauge-5	0.02	0.26

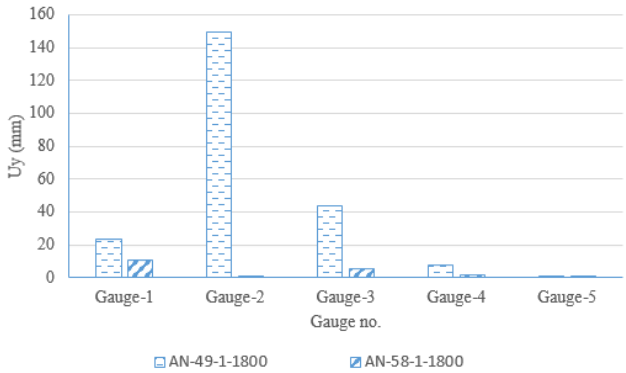

Figure 31. Uy (vertical displacement) of different anchored barriers due to same TNT charge (1800 kg)

Table 3. Uz (horizontal displacement) of different anchored barriers due to same TNT charge (450 kg)

	Max Uz (mm)	
Gauge No.	**AN-49-1-450**	**AN-58-1-450**
Gauge-1	-91.75	-24.02
Gauge-2	-74.81	-43.99
Gauge-3	-83.46	-54.31
Gauge-4	-82.94	-53.99
Gauge-5	-90.04	-41.79

Moreover, in case of Uz (horizontal displacement) for type-2 barriers the values of AN-49-1-1800 gauges is less than AN-

58-1-1800 gauges by ratios vary between 7.60% up to 120.60% at different gauges except gauge (2). Also, the results of Uz are shown in Table 4. Furthermore, Figure 33 compares the results of Uz at different gauges for AN-49-1-1800 and AN-58-1-1800.

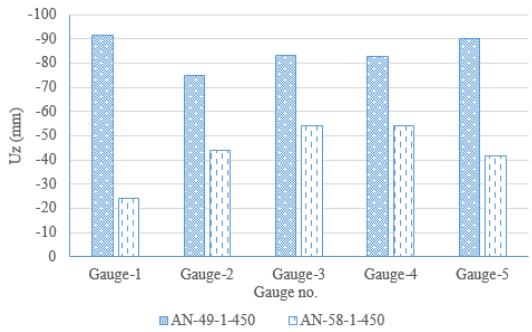

Figure 32. Uz (horizontal displacement) of different anchored barriers due to same TNT charge (450 kg)

Table 4. Uz (horizontal displacement) of different anchored barriers due to same TNT charge (1800 kg)

	Max Uz (mm)	
Gauge No.	**AN-49-1-1800**	**AN-58-1-1800**
Gauge-1	-44.02	-62.21
Gauge-2	-428.70	-280.94
Gauge-3	-219.38	-235.95
Gauge-4	-16.37	-36.12
Gauge-5	-8.30	-10.38

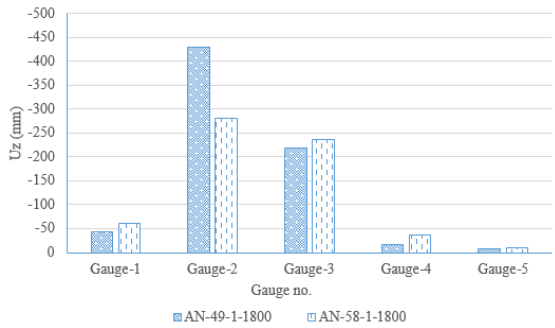

Figure 33. Uz (horizontal displacement) of different anchored barriers due to same TNT charge (1800 kg)

In addition, in case of Uy (vertical displacement) for type-3 barriers the values of EM-58-1-450 gauges is less than EM-49-1-450 gauges by ratios from 44% up to 99% at different gauges except gauge (1) and (5). Furthermore, Table 5 display the results of Uy and Figure 34 compares the results of Uy at different gauges for EM-49-1-450 and EM-58-1-450.

Table 5. Uy (vertical displacement) of different embedded barriers due to same TNT charge (450 kg)

	Max Uy (mm)	
Gauge No.	**EM-49-1-450**	**EM-58-1-450**
Gauge-1	0.00	0.00
Gauge-2	18.40	2.88
Gauge-3	15.90	8.90
Gauge-4	20.04	0.27
Gauge-5	0.00	0.35

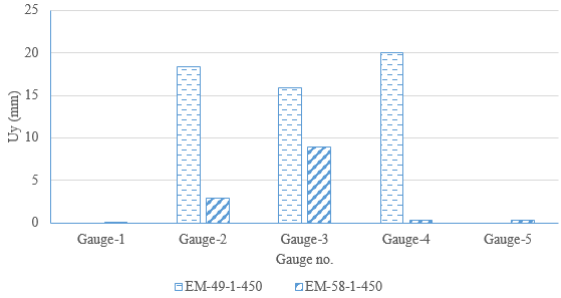

Figure 34. Uy (vertical displacement) of different anchored barriers due to same TNT charge (450 kg)

Furthermore, in case of Uy (vertical displacement) for type-4 barriers the values of EM-58-1-1800 gauges is less than EM-49-1-1800 gauges by ratios more than 100% at different gauges except gauge (1) and (5). The results of Uy are illustrated in Table 6. Furthermore, Figure 35 compares the results of Uy at different gauges for EM-49-1-1800 and EM-58-1-1800.

Moreover, in case of Uz (horizontal displacement) for type-3 barriers the values of EM-58-1-450 gauges is less than EM-49-1-450 gauges by ratios vary between 23.90% up to 81.40% at different gauges. Also, Table 7 shows the results of Uz and Figure 36 represent comparison between gauges for EM-49-1-450 and EM-58-1-450.

Table 6. Uy (vertical displacement) of different embedded barriers due to same TNT charge (1800 kg)

	Max Uy (mm)	
Gauge No.	**EM-49-1-1800**	**EM-58-1-1800**
Gauge-1	-20.40	-6.46
Gauge-2	0.00	-42.13
Gauge-3	0.00	-20.41
Gauge-4	0.00	-1.03
Gauge-5	-2.52	-1.62

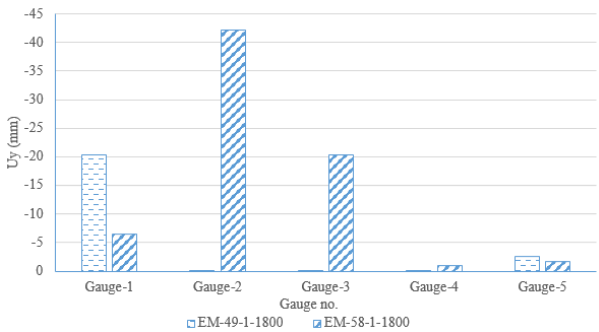

Figure 35. Uy (vertical displacement) of different anchored barriers due to same TNT charge (1800 kg)

Table 7. Uz (horizontal displacement) of different embedded barriers due to same TNT charge (450 kg)

	Max Uz (mm)	
Gauge No.	**EM-49-1-450**	**EM-58-1-450**
Gauge-1	-18.90	-3.52
Gauge-2	-100.05	-76.04
Gauge-3	-107.17	-73.62
Gauge-4	-105.47	-74.84
Gauge-5	-21.94	-5.81

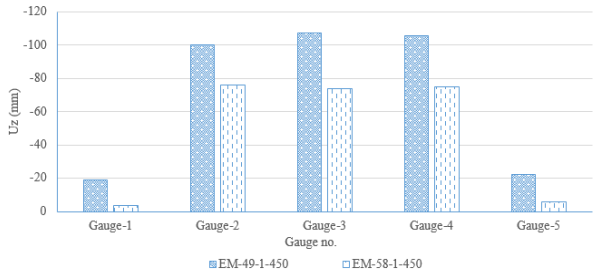

Figure 36. Uz (horizontal displacement) of different anchored barriers due to same TNT charge (450 kg)

Table 8. Uz (horizontal displacement) of different embedded barriers due to same TNT charge (1800 kg)

	Max Uz (mm)	
Gauge No.	**EM-49-1-1800**	**EM-58-1-1800**
Gauge-1	-38.58	-17.34
Gauge-2	-443.73	-297.68
Gauge-3	-78.81	-59.83
Gauge-4	-14.48	-15.54
Gauge-5	-10.12	-10.46

Also, in case of Uz (horizontal displacement) for type-4 barriers the values of EM-58-1-1800 gauges is less than EM-49-1-1800 gauges by ratios vary between 24.10% up to 55.10% at different gauges except guage (4) and (5). The results of Uz are discussed in Table 8. Moreover, Figure 37 compares the results of Uy at different gauges for EM-49-1-1800 and EM-58-1-1800.

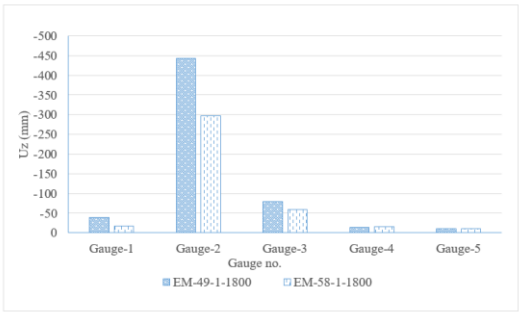

Figure 37. Uz (horizontal displacement) of different anchored barriers due to same TNT charge (1800 kg)

7. CONCLUSIONS

The previous results can be discussed from various perspective, such as pressure values behind barriers as the less values of pressures indicate better protection for people and important buildings. In addition, from the displacement point of view, the values can be compared as the least displacement values indicate better performance of barrier.

7.1 From pressure perspective

In case of anchored barriers:

1. The best performance behind the RC barrier according to the pressure values of gauges 4, 5, 6 is for barriers with front angle 49°, in case of 450 kg. It worth to mention that pressure values behind barriers of AN-49-450 are less than AN-58-450 with ratio varies between 6.50% up to 61% except gauge (6).

2. In case of 1800 kg the best performance is for barriers with front angle 58°. Moreover, pressure values behind barriers of AN-58-1800 are less than AN-49-1800 with ratio varies between 1.00% up to 21.80% except gauge (6).

In case of embedded barriers:

1. In case of 450 kg and 1800 kg the best performance was for barriers with front angle 58°. Also, pressure values behind barriers of EM-58-1800 are less than EM-49-1800 with ratio varies between 2.30% up to 52.60% except gauge (5).

7.2 From displacement perspective

In case of anchored barriers:

As discussed in details at the results section, the following is concluded:

1. For charge 450 kg, the best performance was for barriers with front angle 58°. The displacements values of AN-58-1-450 gauges is less than AN-49-1-450 gauges by ratios vary between 3.50% up to 82.90%.

2. For charge 1800 kg, it can be observed that in vertical Y-direction, the best performance is for barriers with front angle 58°. The values of vertical displacement of AN-58-1-1800 gauges are less than AN-49-1-1800 gauges by ratios vary between 54.20% up to 87.10%. On the contrary, at horizontal Z-direction, the best performance is for barriers with front angle 49°. horizontal displacement for barriers AN-49-1-1800 gauges is less than AN-58-1-1800 gauges by ratios vary between 7.60% up to 120.60%.

In case of embedded barriers:

1. For charge 450 kg and 1800 kg the best performance is for barriers with front angle 58°. The horizontal and vertical displacement values of barriers with front angle 58° less than barriers with front angle 49° by ratios vary between 24.10% up to more than 100%.

2. It worth to mention also that the main reason of failure of walls is crushing of concrete due to the high pressure results from blast load, as the higher weights of TNT charges leads to severe damage of barrier as it is noticed from previous pressure graphs.

3. Furthermore, it can be observed that the pressure values and damage in concrete in case of embedded barriers is higher than the anchored barriers.

4. Current study can be used widely to enhance the performance of barriers using two approaches either anchoring the wall into base or embedding the base into soil.

5. Both approaches are economic and practical. In addition, both approaches don't need high technology or intensive labor.

ACKNOWLEDGMENT

The researcher extends her gratitude to everyone who contributed any information to the research.

REFERENCES

[1] Wu, Y., Wang, J., Liu, F., Mu, C., Xia, M., Yang, S. (2023). A research investigation into the impact of reinforcement distribution and blast distance on the blast resilience of reinforced concrete slabs. Materials, 16(11): 4068. http://doi.org/10.3390/ma16114068

[2] Mai, V.C., Vu, N.Q., Nguyen, V.T, (2020). Ultra-high Performance Fiber Reinforced Concrete panel subjected

to severe blast loading. Defense Science Journal, 70(6): 603-611. http://doi.org/10.14429/dsj.70.15835
[3] Park, Y., Kim, K., Park, S.W., Yum, S.G., Baek, J.W. (2024). Experimental evaluation on blast resistance of reinforced concrete structures under partially confined explosion. International Journal of Concrete Structures and Materials, 18(1): 34. https://doi.org/10.1186/s40069-024-00663-2
[4] Attia, W., Elwan, S., Kotb, I. (2021). Investigating the effect of the geometry of RC barrier walls on the blast wave propagation. International Journal of Safety and Security Engineering, 11(3): 255-268. http://doi.org/10.18280/ijsse.110306
[5] UFC 3-340-02. (2008). Unified facilities criteria (UFC) structures to resist the effects of accidental explosions. US Department of Army, Navy and Air Force, Washington DC. https://www.wbdg.org/FFC/DOD/UFC/ARCHIVES/ufc_3_340_02.pdf.
[6] Sadovsky, M.A. (2004). Mechanical effects of air shockwaves from explosions according to experiments. Geophysics and Physics of Explosion (ed. MA Sadovsky), Nauka Press, Moscow. https://www.abebooks.com/9785020329607/Selected-works-Geophysics-Physics-Explosion-5020329606/plp.
[7] Krauthammer, T., Altenberg, A. (2000). Negative phase blast effects on glass panels. International Journal of Impact Engineering, 24(1): 1-17. http://doi.org/10.1016/S0734-743X(99)00043-3
[8] Hopkinson, B. (1915). British ordnance board minutes 13565. The National Archives, UK. https://scholar.google.com/scholar?q=Hopkinson+B+1915+British+Ordnance+Board+Minutes+%28London%3A+British+Ordnance+Office%29+Report+13565.
[9] Cranz, C., Poppenberg, Eberhard, O.V. (1926). Lehrbuch der Ballistik, Zweiter Band-Innere Ballistik. Verlag Julius Springer, Berlin. https://doi.org/10.1007/978-3-642-52612-1
[10] Hung, C.W., Tsai, Y.K., Chien, L.K., Pi, S.J. (2024). Numerical study of a near-field explosion using arbitrary Lagrangian–Eulerian mapping technique. International Journal of Protective Structures, 15(2): 316-336. http://doi.org/10.1177/20414196231166067
[11] Jindra, D., Hradil, P., Kala, J. (2024). Finite element analysis of concrete slab exposed to high velocity pressure wave - simplified vs. smoothed-particle hydrodynamics (SPH) method. MATEC Web of Conferences. 396: 05005. http://doi.org/10.1051/matecconf/202439605005
[12] Riedel, W., Kawai, N., Kondo, K.I. (2009). Numerical assessment for impact strength measurements in concrete materials. International Journal of Impact Engineering, 36(2): 283-293. https://doi.org/10.1016/j.ijimpeng.2007.12.012
[13] Johnson, G.R., Cook, W.H. (1985). Fracture characteristics of three metals subjected to various strains, strain rates, temperatures and pressures. Engineering Fracture Mechanics, 21(1): 31-48. http://doi.org/10.1016/0013-7944(85)90052-9
[14] Lee, E., Finger, M., Collins, W. (1973). JWL equation of state coefficients for high explosives (No. UCID-16189). Lawrence Livermore National Lab. (LLNL), Livermore, CA (United States). https://doi.org/10.2172/4479737
[15] Farag, G., Chinnayya, A. (2024). On the Jones-Wilkins-Lee equation of state for high explosive products. Propellants, Explosives, Pyrotechnics, 49(3): e202300223. http://doi.org/10.1002/prep.202300223
[16] Castedo, R., Natale, M., López, L.M., Sanchidrián, J.A., Santos, A.P., Navarro, J., Segarra, P. (2018). Estimation of Jones-Wilkins-Lee parameters of emulsion explosives using cylinder tests and their numerical validation. International Journal of Rock Mechanics and Mining Sciences, 112: 290-301. http://doi.org/10.1016/j.ijrmms.2018.10.027
[17] Mavko, G., Mukerji, T., Dvorkin, J. (2020). The rock physics handbook. Cambridge University Press. http://doi.org/10.1017/9781108333016
[18] Alejano, L.R., Bobet, A. (2012). Drucker–Prager criterion. Rock Mechanics and Rock Engineering, 45: 995-999. http://doi.org/10.1007/s00603-012-0278-2
[19] Chen, J.Y., Feng, D.L., Liu, J.H., Yu, S.Y., Lu, Y. (2023). Numerical modeling of the damage mechanism of concrete-soil multilayered medium subjected to underground explosion using the GPU-accelerated SPH. Engineering Analysis with Boundary Elements, 151: 265-274. http://doi.org/10.1016/j.enganabound.2023.03.003
[20] Bomb Threat Standoff Distance Chart. (2010). Office of the director of National Intelligence, National Counter Terrorism Center (NCTC). U.S. Department of Homeland Security. https://www.dni.gov/nctc/jcat/references.html.

NOMENCLATURE

Z	The scaled distance, (m. $kg^{1/3}$)
R	The range from the center of the charge, (m)
W	The mass of TNT charge, (kg)
P	Pressure, (MPa)
t	Time, (s)
P_o	Ambient pressure, (MPa)
P_{so}	Positive peak pressure, (MPa)
P^-_{so}	Negative peak pressure, (MPa)
t_{pos}	The time duration of positive overpressure, (s)
t_{neg}	The time duration of negative overpressure, (s)

Subscripts

so	positive overpressure
pos	positive
neg	negative